Mem. Fac. Sci. Eng. Shimane Univ.
Series A
38, pp.17-24 (2004)

Deformation analysis of clay foundation under embankment using non-coaxial Cam-clay model

Toshihide SHIBI and Takeshi KAMEI
Department of Geoscience, Interdisciplinary Faculty of Science and Engineering, Shimane University

Abstract

In this paper, the deformation behavior of the soft ground using a non-coaxial Cam-clay model under an embankment fill has been simulated by deformation analysis using a finite element method. The results of deformation analysis using the non-coaxial Cam-clay model have been compared with those using a coaxial Cam-clay model. The results show clear transition from localized strain to formation of a circular arc band in which maximum shear strain is localized, as demonstrated by deformation analysis using a non-coaxial Cam-clay model. Using the non-coaxial Cam-clay model, the circular arc band is clearly formed in the embankment foundation at an earlier stage of embankment construction than that using the coaxial Cam-clay model. Based on these results, it is suggested that estimation of foundation deformation using the non-coaxial Cam-clay model is superior to that using the coaxial Cam-clay model. The deformation analytical results provide significant information for construction management of geotechnical projects and prediction of slope failures by using the non-coaxial Cam-clay model.

1. Introduction

Vertical and horizontal deformations for foundations under embankments are often large, and are potentially damaging to structures. Embankment fill applies vertical load to the foundation surface in combination with an outward shear stress caused by horizontal stresses in the fill. Evaluating their magnitude plays an important part in many geotechnical engineering projects. Deformation analysis of the clay foundation under embankments is also required for embankment design. This deformation analysis becomes increasingly important when embankments are constructed over weak material (normally consolidated cohesive stratum). In these situations, as a consequence of the widespread use of powerful computers and theoretical soil mechanics over the last few decades, it has been become possible to carry out sophisticated numerical analysis. Consequently, the results of numerical simulation can be assessed qualitatively and quantitatively by comparison with field-measured data (e. g. Sakajo and Kamei, 1995, 1996; Kamei and Sakajo, 1998).

The original Cam-clay model developed by Roscoe et al. (1963) provides a reasonable match to the experimentally observed behavior of saturated clay using only four soil parameters. This model is a coaxial hardening elasto-plastic model up to a critical state: the principal directions of incremental plastic strains are coaxial with those of current stresses. In the Cam-clay model, incremental stresses make no contribution to the principal directions of incremental plastic strains.

The localization of deformation into a shear band for pressure-sensitive dilatant material is not explained by the flow theory of plasticity, which is based on the assumption of coaxiality between the principal directions of incremental plastic strain and those of current stress. This restriction in the flow theory has been relaxed by Rudnicki and Rice (1975), who considered the contribution of a non-coaxial term persuaded by arguments in favor of a yield vertex plasticity. Papamichos and Vardoulakis (1995) suggested a similar modification to the flow theory of an elastic-plastic model for sand. Yatomi et al. (1989a) proposed a non-coaxial Cam-clay model, simply following the basic procedure of Rudnicki and Rice (1975). The incorporation of the non-coaxial term into a constitutive model has no effect on the instantaneous shear modulus for the normal stress difference, but makes the instantaneous shear modulus for shear stress smaller. In the theoretical prediction of shear band formation, a non-coaxiality influences the shear band inclination angle, and facilitates shear band formation. In contrast, non-coaxiality arising from the anisotropy does not contribute much to triggering instability by localization of the deformations which result in shear band formation, whereas the non-coaxiality due to the yield vertex effect is inclined towards instability by localization of the deformations (Iizuka et al., 1992). Bifurcation analysis in a circular cylindrical

specimen using the non-coaxial Cam-clay model was carried out. Incorporation non-coaxiality made bifurcation phenomenon occur easily, and explained the patterns of slip planes observed in the triaxial test of saturated clays (Yatomi and Shibi, 1997). Yatomi et al. (1989b) carried out finite element analysis for finite strain in a classical rigid punch problem without introducing any initial imperfections into the material elements, and as a result obtained a deformation of shear band formation.

This paper investigates the influence of incorporating non-coaxiality into a constitutive model for clay on deformation analytical results of soft ground under an embankment fill. Deformation behavior of the soft ground using a non-coaxial Cam-clay model under an embankment fill has been simulated by deformation analysis using a finite element method. The results of the deformation analysis using the non-coaxial Cam-clay model are compared with those using a coaxial Cam-clay model. The results show that deformation analysis using a non-coaxial Cam-clay model provides clear transition from localized strain to formation of shear band. Based on these results, the utility of incorporating non-coaxiality into a clay model for deformation analysis is discussed.

2. Constitutive relation

In this paper, we employ the original coaxial Cam-clay model and a second model (a non-coaxial Cam-clay model) which incorporates a non-coaxial term. These constitutive models are summarized briefly below:

The yield function of the Cam-clay model is of the type

$$F = f(q, p', p'_0) - v^{\mathrm{p}} = 0\,, \tag{1}$$

where the mean effective stress p' and the generalized stress deviator q are defined as

$$p' = \frac{1}{3}\sigma'_{ii}\,,\quad q = \sqrt{\frac{3}{2}S_{ij}S_{ij}}\,, \tag{2}$$

and p'_0 is the mean effective stress at the initial state, and v^{p} is the volumetric plastic strain. Here, σ'_{ij} is the effective stress and S_{ij} is the deviatoric part of σ'_{ij}. Equation (1) is fully expressed as

$$F = \frac{\lambda-\kappa}{1+e_0}\ln\frac{p'}{p'_0} + D\frac{q}{p'} - v^{\mathrm{p}} = 0\,, \tag{3}$$

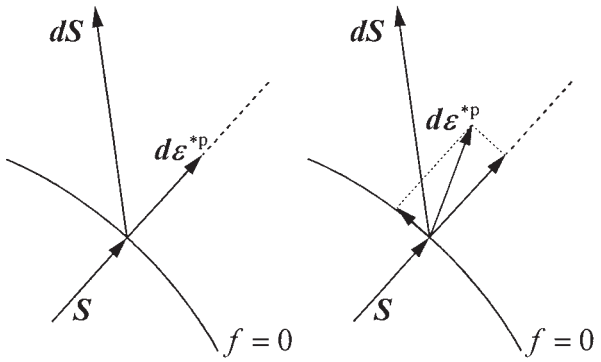

(a) Coaxial model (b) Non-coaxial model

Figure 1 Deviatoric part of incremental plastic strain for coaxial and non-coaxial models

where λ and κ are the compression index and the swelling index respectively, e_0 is the void ratio at the initial state, p'_0 is the mean effective stress at the initial state, and D is the coefficient of dilatancy, which is related to the critical state parameter M as defined by $D=(\lambda-\kappa)/\{M(1+e_0)\}$ (e. g. Shibata, 1963; Sekiguchi and Ohta, 1977; Kamei, 1989).

The plastic part of incremental strain $d\varepsilon^{\mathrm{p}}_{ij}$ is expressed by a coaxial flow theory as

$$2d\varepsilon^{*\mathrm{p}}_{ij} = \frac{1}{h}\frac{S_{ij}}{\bar{\tau}}\left(\frac{S_{k\ell}}{2\bar{\tau}}d\sigma'_{k\ell} + \frac{1}{3}\bar{\beta}d\sigma'_{kk}\right)\,, \tag{4a}$$

$$d\varepsilon^{\mathrm{p}}_{kk} = \frac{\bar{\beta}}{h}\left(\frac{S_{k\ell}}{2\bar{\tau}}d\sigma'_{k\ell} + \frac{1}{3}\bar{\beta}d\sigma'_{kk}\right) \tag{4b}$$

with $\bar{\tau} = \sqrt{S_{ij}S_{ij}/2}$ and $\bar{\beta} = (M - q/p')/\sqrt{3}$, where $d\varepsilon^{*\mathrm{p}}{}_{ij}$ is the deviatoric part of $d\varepsilon^{\mathrm{p}}_{ij}$, $d\sigma_{ij}$ is the incremental effective stress, and h is the hardening modulus given by

$$h = \frac{p'\bar{\beta}}{\sqrt{3}D}\,. \tag{5}$$

Yatomi et al. (1989a) called the above constitutive relations the coaxial Cam-clay model because the principal directions of $d\varepsilon^{*\mathrm{p}}{}_{ij}$ are coaxial with the principal directions of S_{ij} (see, Fig. 1(a)).

The coaxial Cam-clay constitutive relation is expressed as

$$d\sigma'_{ij} = \{(\tilde{K} - \frac{2}{3}\tilde{G})\delta_{ij}\delta_{k\ell} + \tilde{G}(\delta_{ik}\delta_{j\ell} + \delta_{i\ell}\delta_{jk}) - \frac{1}{\tilde{G}+\tilde{h}}\left(\frac{\tilde{G}}{\bar{\tau}}S_{ij} + \tilde{K}\bar{\beta}\delta_{ij}\right)\left(\frac{\tilde{G}}{\bar{\tau}}S_{k\ell} + \tilde{K}\bar{\beta}\delta_{k\ell}\right)\}d\varepsilon_{k\ell}\,, \tag{6}$$

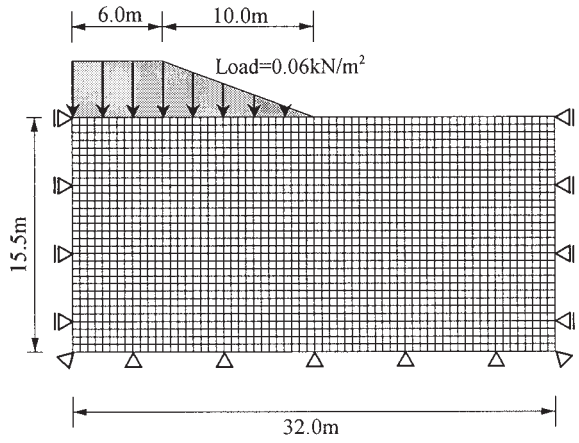

Figure 2 Finite element mesh used in the present study

where $\tilde{K}(=(1+e)p'/\kappa)$ is the bulk modulus and $\tilde{G}(=3(1-2\nu)\tilde{K}/\{2(1+\nu)\})$ is the shear modulus, where ν is Poisson's ratio.

The deviatoric part of incremental plastic strain $d\varepsilon^{*p}_{ij}$ is expressed by a non-coaxial flow theory (Rudnicki and Rice, 1975) of the form

$$2d\varepsilon^{*p}_{ij} = \frac{1}{h}\frac{S_{ij}}{\bar{\tau}}\left(\frac{S_{k\ell}}{2\bar{\tau}}d\sigma'_{k\ell} + \frac{1}{3}\bar{\beta}d\sigma'_{kk}\right) + \frac{1}{h_1}\left(dS_{ij} - \frac{S_{ij}S_{k\ell}}{2\bar{\tau}^2}dS_{k\ell}\right) \quad (7)$$

Here h_1 is the second hardening modulus, which was, for simplicity, assumed by Yatomi et al. (1989a) to have similar form as the hardening modulus h as

$$h_1 = \frac{p'\bar{\beta}}{\sqrt{3}A}(>0), \quad (8)$$

where A (the non-coaxial parameter) is a positive material constant. The additional term to $d\varepsilon^{*p}_{ij}$ is the tangential direction of yield surface in Fig. 1(b). The additional term $d\varepsilon^{*p}_{ij}$ is workless and thus makes no contribution to the rate of plastic energy loss. The effect of incorporating the non-coaxial term is merely exchanging the coefficients in Eq. (6) as

$$\tilde{G} \to \frac{h_1\tilde{G}}{h_1+\tilde{G}}, \quad \tilde{K} \to \frac{(h_1-h)\tilde{K}}{h_1-h-\bar{\beta}^2\tilde{K}}, \quad h \to \frac{h_1 h}{h_1-h},$$
$$\text{and} \quad \bar{\beta} \to \frac{h_1\bar{\beta}}{h_1-h}. \quad (9)$$

Table 1 A set of soil parameters used in the present study (Sekiguchi, 1977; Yatomi et al., 1989a)

λ	=	0.231
κ	=	0.042
ν	=	0.333
e_0	=	1.5
M	=	1.43
A	=	0.01 (0) *

*A=0.01 for the non-coaxial Cam-clay model, and A=0 for the coaxial Cam-clay model

When the principal directions of dS_{ij} correspond with the principal directions of S_{ij}, the additional term to $d\varepsilon^{*p}_{ij}$ is zero, and incorporating the non-coaxial term consequently has no effect on $d\varepsilon^{p}_{ij}$ in this case.

3. Finite element analysis, boundary conditions and their modeling

The finite element program used in this study was coded according to the method proposed by Sandhu and Wilson (1969). The type of solid element used for deformation was a second order iso-parametric plane-strain element with 8 nodal points, and a first order iso-parametric element with 4 nodal points was used for pore water pressure. An embankment foundation with 1984 elements (6143 nodal points; Fig .2) was modeled to investigate the influence of incorporating non-coaxiality into a constitutive model for clay on deformation analytical results of soft ground under an embankment fill. The finite element array and the boundary conditions are also shown in Fig. 2. The targeted analytical area was symmetrical about the centerline, so the mesh represents half the cross-section through the cutting. Embankment load was expressed by the distribution load. The simulation was carried out until the embankment load reached that corresponding an embankment height of 4.0m. Short term stability is one of the most important problems for construction on weak cohesive soils so the embankment fill was rapidly constructed.

The model embankment was constructed on a 15m deep model foundation of cohesive soils. A 50cm thick sand mat was first placed on the original surface of the weak cohesive soil before embankment construction began. Bedrock was located at a depth of 15.5m. The cohesive soil foundation was in a normally consolidated state. The soil parameters of the foundation (Table 1) were determined from experimental results from triaxial tests on Umeda Clay, as reported by Sekiguchi (1977). The remaining parameters of the model

were assumed to be: coefficient of permeability for clay k = 1.0 x 10^{-9}m/s; shear modulus for sand E_s = 3600kN/m^2; Poisson's ratio for sand ν_s = 0.45; coefficient of permeability for sand k_s = 1.0 x 10^{-5}m/s. The intensity of non-coaxiality of clay was not experimentally investigated. However, non-coaxiality is very important for theoretical explanation of the deformation behavior of clay, which is accompanied by bifurcation phenomenon (Yatomi and Shibi, 1997). In this paper, we estimated a non-coaxial parameter from the results based on the theory of shear band formation using the non-coaxial Cam-clay model (Yatomi et al., 1989a) and the numerical results of bifurcation analysis using the non-coaxial Cam-clay model (Shibi et al., 2000).

For the boundary condition, horizontal displacements were fixed along the vertical line at the center of the embankment and at the right side of the foundation. Both the horizontal and vertical displacements were fixed along the bottom line of the foundation. With respect to drainage condition, the model assumed complete drainage along the ground surface and the bottom line of the foundation. The boundary along the vertical line at the center of the embankment and the right side of foundation was set as impermeable.

4. Deformation analytical results and discussions

The objective of the present deformation analysis is to investigate the utility of incorporating non-coaxiality into a clay model in the deformation analysis of embankment foundation.

A process of deformation of embankment foundation using the non-coaxial Cam-clay model is shown in Fig. 3. In the early stage of embankment construction (embankment height = 2.8m), the amount of ground surface settlement was the same from the center of the embankment to the embankment shoulder, and decreased while from the shoulder to the embankment toe. The ground surface in front of the embankment toe heaved slightly. Displacement in the ground was about 15cm at most. The amount of ground surface settlement under the embankment shoulder was slightly larger than that at the center of embankment when the embankment height reached 3.4m, and slight shear deformation appeared in the elements under the embankment shoulder. The difference of the amount of the ground surface settlement between the shoulder and the center of the embankment extended as embankment height increased beyond 3.4m. The shear deformation in the element under the embankment shoulder became greater than any other element when the embankment height reached 3.8m. When the embankment height finally

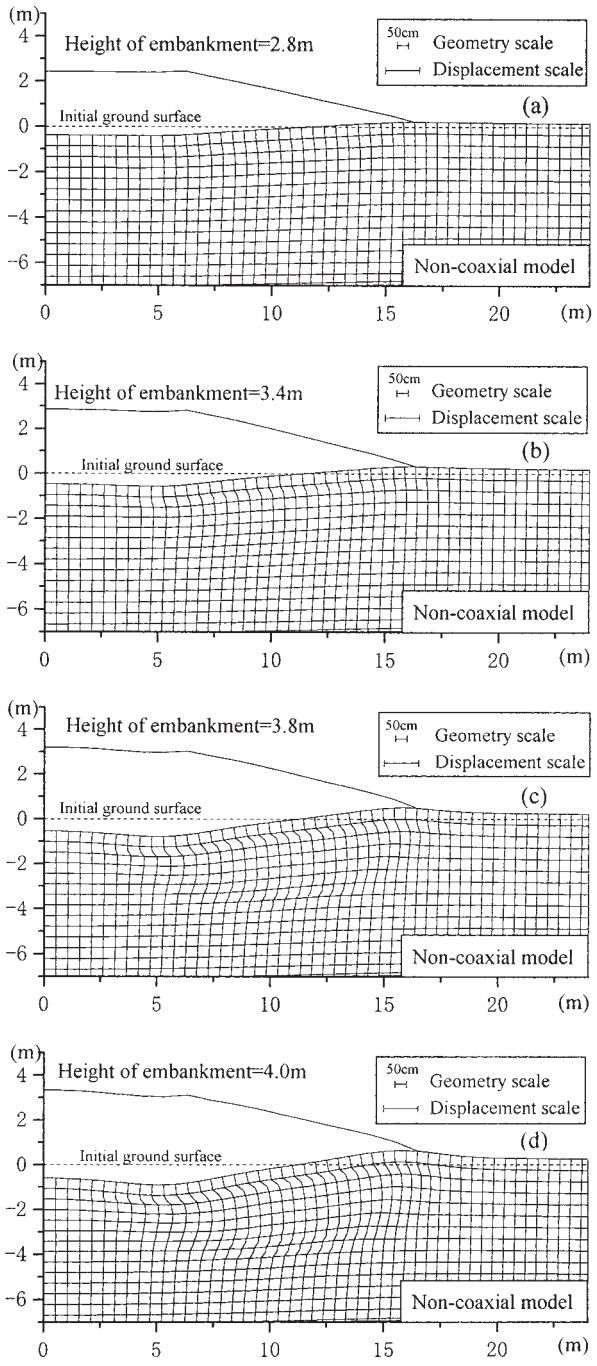

Figure 3 Embankment foundation deformations using the non-coaxial Cam-clay model

reached 4.0m, the area occupied by the element with marked shear deformation extended from the embankment shoulder to the toe in a circular arc band. This circular arc reached about 4m in depth.

Ground surface subsided uniformly with increasing embankment height up to the embankment height of 2.8m. In this case, the embankment foundation stably deformed and consolidation was responsible for the majority of the

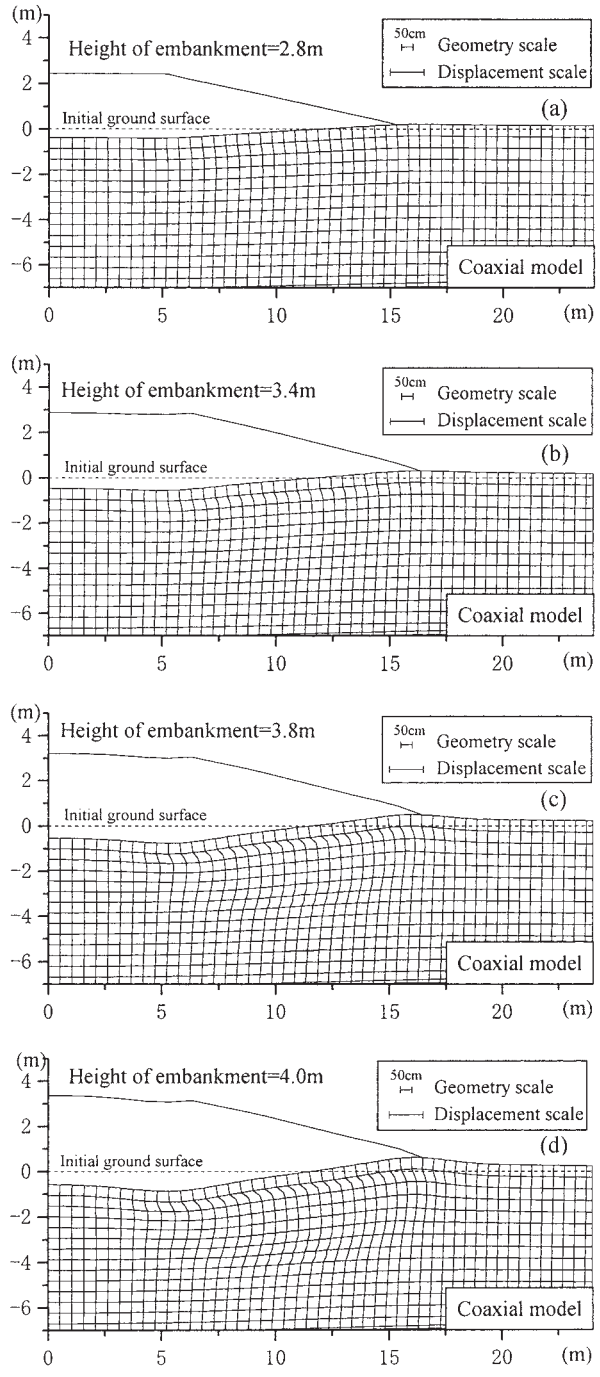

Figure 4 Embankment foundation deformations using the coaxial Cam-clay model

deformation in the embankment foundation. Settlement of ground surface, however, locally progressed beneath the embankment shoulder when the embankment height exceeded 2.8m. This settlement of the ground surface is related to localization of shear deformation in the elements beneath the embankment shoulder, and is one of the signs of failure of embankment foundations. The area of localized deformation extended in front of the embankment when the embankment height passed 3.4m.

The process of deformation of embankment foundation using the non-coaxial Cam-clay model is compared with those using the coaxial Cam-clay model. Fig. 4 shows the process of deformation of embankment foundation using the coaxial Cam-clay model. The process using the non-coaxial Cam-clay model almost corresponded with those using the coaxial Cam-clay model up to an embankment height of 3.4m. However, when the embankment height reached 3.8m, the shear deformation of elements using the non-coaxial Cam-clay model under the embankment shoulder was more significant than that using the coaxial Cam-clay model. The difference between the settlement under the shoulder using the non-coaxial Cam-clay model and that using the coaxial Cam-clay model increased as the embankment height rose. The shape of the circular arc band occupied by the element with marked shear deformation using the non-coaxial Cam-clay model almost corresponded to that using the coaxial Cam-clay model when the embankment height reached 4.0m. The degree of shear deformation in this band, however, was more marked using the non-coaxial Cam-clay model than using the coaxial Cam-clay model.

Propagation of failure of embankment foundation can be seen more clearly in the strain distribution. Contours of maximum shear strain using the non-coaxial Cam-clay model are shown in Fig. 5.

Maximum shear strain slightly increased at first in a small area beneath the embankment shoulder reaching maximum shear strain of 2-4% when embankment height reached 2.8m (Fig. 5(a)). When the embankment height reached 3.4m, the area of higher maximum shear strain extended from the embankment shoulder to the embankment toe in a circular arc which reached a depth of about 4m (Fig. 5(b)). A slight maximum in shear stain was computed in the area about 1m beneath the embankment. In this area, depth was shallow and consequently the shear strength was small and small loading yielded large strain. On the other hand, this slight maximum shear strain was formed by lateral outward movement of the embankment foundation at depths in excess of 1m (see Fig. 3). Therefore, the slight maximum shear strain in this area scarcely influenced outward lateral movement at depths in excess of 1m. When embankment height exceeded 3.8m, maximum shear strain increased locally in a circular arc band (Fig. 5(c)). Maximum shear strain in the arc band increased to 6-8% at 3.8m in embankment height, and reached 8-10% in the final stage at 4.0m embankment height (Fig. 5(d)).

The propagation of failure of embankment foundation using the coaxial Cam-clay model is given in Fig. 6.

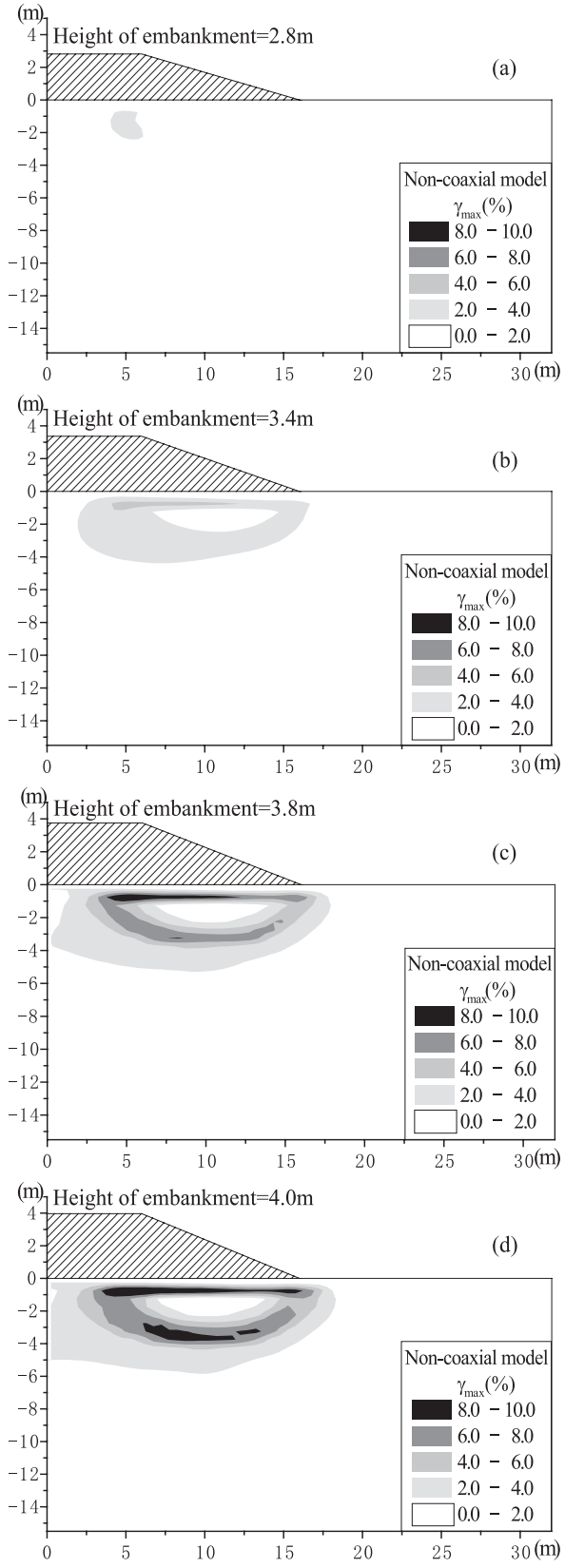

Figure 5 Contours of maximum shear strain using the non-coaxial Cam-clay model

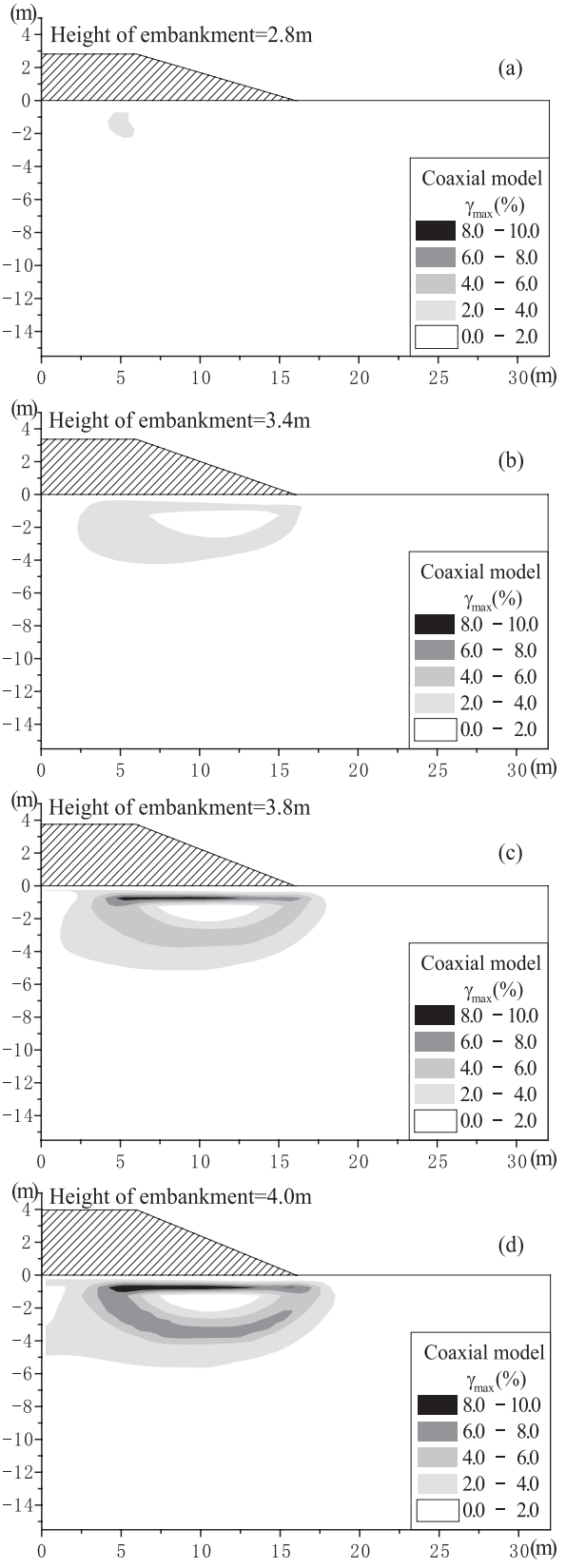

Figure 6 Contours of maximum shear strain using the coaxial Cam-clay model

At 2.8m embankment height, the contour of maximum shear strain using the coaxial model almost corresponds to that using the non-coaxial model (Fig. 6(a)). At 3.4m, the maximum shear stain using the coaxial model was slightly smaller in the area 1m beneath the embankment than that using the non-coaxial model. In both models, however, the area of slightly larger maximum shear strain appeared from the embankment shoulder to the embankment toe in a circular arc (Fig. 6(b)). When embankment height exceeded 3.8m, maximum shear strain in the circular arc band grew later and was less in the coaxial model than with the non-coaxial model (Fig. 6(c)). Both models agree in the shape of the circular arc band (the shear band) in which the maximum shear strain is localized. The amount of maximum shear strain in the shear band at 4.0m in the coaxial model (Fig. 6(d)) nearly matches to that at 3.8m in the non-coaxial model. The difference in the maximum shear strain between the models suggests that deformation analysis using the non-coaxial Cam-clay model may detect signs of failure of embankment foundations at an earlier stage than does the coaxial model. Consequently, deformation analysis using the non-coaxial Cam-clay model yields significant information for construction management of geotechnical projects and prediction of slope failure. Additional study in geotechnical engineering thus seems justified.

5. CONCLUSIONS

The present deformation analysis, which models construction of embankment fill on soft ground using the non-coaxial and coaxial Cam-clay models, demonstrates clear transition from localized strain to formation of shear bands. Incorporating non-coaxiality into a constitutive model for clay shows that marked shear deformation and large maximum shear strain occur under the embankment shoulder in the early stage of embankment construction. However, the area of marked shear deformation and large maximum shear strain almost correspond with that which disregards non-coaxiality.

The present deformation analysis using the non-coaxial Cam-clay model provides significant information for construction management of geotechnical projects and prediction of slope failures. Additional study in geotechnical engineering seems to be justified, however.

ACKNOWLEDGEMENTS

The authors would like to express their gratitude to Dr. B. P. Roser of Shimane University for his careful proofreading of this paper, and to Miss Y. Sakamoto of Gifu city office for her help with computation.

REFERENCES

Iizuka, A., Yatomi, C., Yashima, A., Sano, I. and Ohta, H. (1992): "The effect of stress induced anisotropy on shear band formation," *Archive of Applied Mechanics*, Vol.62, pp.104-114.

Kamei, T. (1989): "Dilatancy characteristics of normally consolidated cohesive soils," *Soils and Foundations*, Vol.29, No.1, pp.165-172.

Kamei, T. and Sakajo, S. (1998): "A deformation analysis of deep foundation under embankment using an elasto-viscoplastic model," *Journal of the Japan Society of Engineering Geology*, Vol.39, No. 2, pp.183-192.

Papamichos, E. and Vardoulakis, I. (1995): "Shear band formation in sand according to non-coaxial plasticity model," *Geotechnique*, Vol.45, No.4, pp.649-661.

Roscoe, K. H., Schofield, A. N. and Thurairajah, A. (1963): "Yielding of clays in states wetter than critical," *Geotechnique*, Vol.13, pp.211-240.

Rudnicki, J. W. and Rice, J. R. (1975): "Conditions for the localization of deformation in pressure-sensitive dilatant materials," *Journal of the Mechanics and Physics Solids*, Vol.23, pp.371-394.

Sakajo, S. and Kamei, T. (1995): "A simple procedure for evaluating deformation characteristics of deep clay foundation under embankment using elasto-plastic model," *Proceedings of the International Symposium on Compression and Consolidation of Clayey Soils*, Hiroshima, Vol.1, pp.739-744.

Sakajo, S. and Kamei, T. (1996): "Simplified deformation analysis for embankment foundation using elasto-plastic model," *Soils and Foundations*, Vol.36, No.2, pp.1-11.

Sandhu, R. S. and Wilson, E. L. (1969): "Finite element analysis of flow in saturated porous media," *Journal of the Engineering Mechanics Division*, ASCE, Vol.95, No.EM3, pp.641-652.

Sekiguchi, H. (1977): "Rheological characteristics of clays," *Proceedings of 9th International Conference on Soil Mechanics and Foundation Engineering*, Tokyo, Vol.1, pp.289-292.

Sekiguchi, H. and Ohta, H. (1977): "Induced anisotropy and time dependency in clays," *Proceedings of 9th International Conference on Soil Mechanics and Foundation Engineering*, Tokyo, Vol.1, pp.229-238.

Shibata, T. (1963): "On the dilatancy of clays," *Disaster Prevention Research Institute*, Kyoto University, No.6, pp.128-134 (in Japanese).

Shibi, T., Kamei, T. and Higashihara, S. (2000): "Influences of Non-coaxial Parameter on Bifurcation Stress Ratio," *Journal of Structures and Materials in Civil Engineering*, No.16, pp.159-167 (in Japanese).

Yatomi, C. and Shibi, T. (1997): "Antisymmetric bifurcation analysis in a circular cylinder of a non-coaxial Cam-clay model,"

Proceedings of the International Symposium Deformation and Progressive Failure in Geomechanics, Nagoya, pp.9-14.

Yatomi, C., Yashima, A., Iizuka, A. and Sano, I. (1989a): "General theory of shear bands formation by a non-coaxial Cam-clay model," *Soils and Foundations*, Vol.29, No.3, pp.41-53.

Yatomi, C., Yashima, A., Iizuka, A., and Sano, I. (1989b): "Shear bands formation numerically simulated by a non-coaxial Cam-clay model," *Soils and Foundations*, Vol.29, No.4, pp.1-13.